RIT

Bubble Nucleation

Vacuum Decay in the Early Universe

Mario L. Gutierrez Abed

Mathematical Modeling I Technical Report 2020

Abstract

In this report we look at the phenomenon of bubble nucleation and decay of a scalar field that posseses a multi-minima potential –one such minimum being a false vacuum and another the true, absolute vacuum state. The project poses both a *computational physics* problem and a *modeling* problem. The former is showcased via a novel computational technique that successfully tackles both the zero-temperature (*instanton*) and finite-temperature (*caloron*) decays, while the modeling component of this project shows both the effect of temperature on vacuum decay and bubble formation and also a (quite mysterious!) link between the height of the potential barrier of the scalar field used in the model and the action of the field. The more surprising bit is not that there is a correlation between these parameters, but rather that this relation is (very!) linear. Previous work on this topic has revealed this strange relation in the 1+1D case. [AM20] Here we show that this linear fit (remarkably) still holds quite well in up to three spatial dimensions.

Contents

CHAPTER 1

Introduction & Theoretical Background

Even though at the very beginning of the existence of our universe the structure of spacetime consisted mostly of large-scale homogeneity with only small-scale perturbative fluctuations, there is plenty of evidence that suggests that, in occasion, non-perturbative effects may have also played an important role during first-order phase transitions. Amongst the latter, the formation and decay of bubbles has been of much interest to the cosmology community ever since the publication of the classical papers by Coleman & Callan ([CC77], [Col77]). Not only do these phase transitions arise in a wide range of hands-on applications such as in the condensation of water vapor and the vacuum decay of fundamental quantum fields, but also, in cosmology, bubbles of a new matter phase are known to produce huge density variations. Thus it is not surprising that first-order phase transitions have been proposed as sources of gravitational waves ([Cap+09; Hin+14]) and as seeds of primordial black holes. [DV17; HMS82] In a cosmological context, the temperature is falling as the universe expands, and at some stage the rate for the first-order phase transition becomes smaller than the rate of vacuum decay.

As proposed in [Bil+19], seeded bubble nucleation can be studied in a laboratory cold-atom analogue of cosmological vacuum decay. [Fia+15] While, traditionally, analogue systems have mostly been employed to test ideas in perturbative quantum field theory, there has been recent interest in using such analogue "table-top" experiments on nonperturbative phenomena such as bubble nucleation. Through "modelling the universe in the lab" we hope to gain a better understanding of the process of vacuum decay and the role of the instanton. This is particularly relevant nowadays in light of the recent measurements of the Higgs mass, which currently indicate that our universe's vacuum is in a region of *metastability*.

In this report we showcase a novel numerical approach to the semiclassical treatment of the false vacuum decay studied in these original papers, with particular interest in the intersection of zero-temperature (vacuum) and finite nonzero-temperature (thermal) nucleation. Both instances are described in terms of an ***instanton***, i.e., a scalar field that is a solution of the imaginary-time classical equations of motion (in the thermal case the field is also usually called a ***caloron***). The motivation for choosing to model an instanton over a classical scalar particle satisfying the Klein-Gordon equation is made clear in Figure 1.2: a classical particle does not penetrate a potential barrier, while an instanton can be used to calculate the transition probability for a quantum mechanical particle to undergo the phenomenon commonly known as *tunneling*, or *barrier penetration*.

1.1 The Model

We are ultimately interested in computing the aforementioned transition probability of tunneling for an instanton. The ***probability of decay*** per unit time per unit volume, Γ/V, of the false vacuum (FV), is given by

$$\Gamma/V = Ae^{-B/\hbar}[1 + \mathcal{O}(\hbar)], \tag{1.1a}$$

where A and B are quantities that reflect the underlying physics. As in the rest of this report, we are using geometrized units ($\hbar = c = k_B = 1$),[1] so we may write (1.1a) as

$$\Gamma/V \approx Ae^{-B}. \tag{1.1b}$$

A numerical treatment of the coefficient B is the focus of the present work. The model for this coefficient is based on the spinor *Bose-Einstein condensate* (BEC) system proposed by [Fia+15], where the relative phase between the wave-functions of two atomic states ϕ is described by the total Euclidean action $S_E = iS$:

$$B = S_E = \int \left[\frac{1}{2}\mathring{\nabla}^a\phi\mathring{\nabla}_a\phi + U(\phi)\right] \mathrm{d}\tau\, \mathrm{d}\vec{x}. \tag{1.2}$$

Here the scalar field $\phi = \phi(\tau, \vec{x})$ is the instanton, which varies in the spatial coordinates $\vec{x}$ and *imaginary time* $\tau = it$, and $\mathring{\nabla}_a\phi$ is the spatial gradient $D_a\phi$ plus the τ-gradient (in Cartesian coordinates, $\mathring{\nabla}_a\phi = \partial_\tau\phi + \partial_{\vec{x}}\phi$). Note also that the Einstein summation convention is being used. Meanwhile the quantity U is a multi-minima potential; in our model we set

$$U(\phi) = \frac{1}{2}\lambda^2 \sin^2\phi - \cos\phi - 1, \tag{1.3}$$

which exhibits a ***false vacuum*** at $\phi_{\mathrm{FV}} \equiv \pi$ and the ***true vacuum*** at $\phi_{\mathrm{TV}} \equiv 0$ (see Fig. (1.2)). The parameter λ has the effect of increasing/decreasing the height of the potential barrier that separates the false and true vacua, and will play a major role in our investigation. We shall illustrate in the later on the conspicuously linear relation it has with the Euclidean action given by Eq. (1.2). As we will see, this link between λ and the action will also imply a dependence of λ on temperature in the thermal case. In an early universe setting, this effect plays an important role in placing the field in the false vacuum as the universe supercools. Moreover, we will suppose that at zero temperature the potential barrier is still present, so in this case the temperature dependence of the potential plays less of a role and we will take λ to be constant.

We point out that, since there may be multiple field solutions $\{\phi_i\}$ that satisfy the field equations, we must sum the contributions to Γ/V of all such fields. At non-zero temperature,

$$\mathcal{Z} = \mathrm{Tr}(e^{-\beta H}) = \int D\phi\, e^{-S_E[\phi]}, \tag{1.4}$$

where Tr denotes a *trace* over all quantum states, H is a *Hamiltonian operator*, and

$$\beta \equiv \frac{k_B}{\hbar T} = \frac{1}{T} \qquad (T = \text{temperature}). \tag{1.5}$$

[1] Furthermore, we are also ignoring gravitational effects. Thus we will be working exclusively with a flat Riemannian metric.

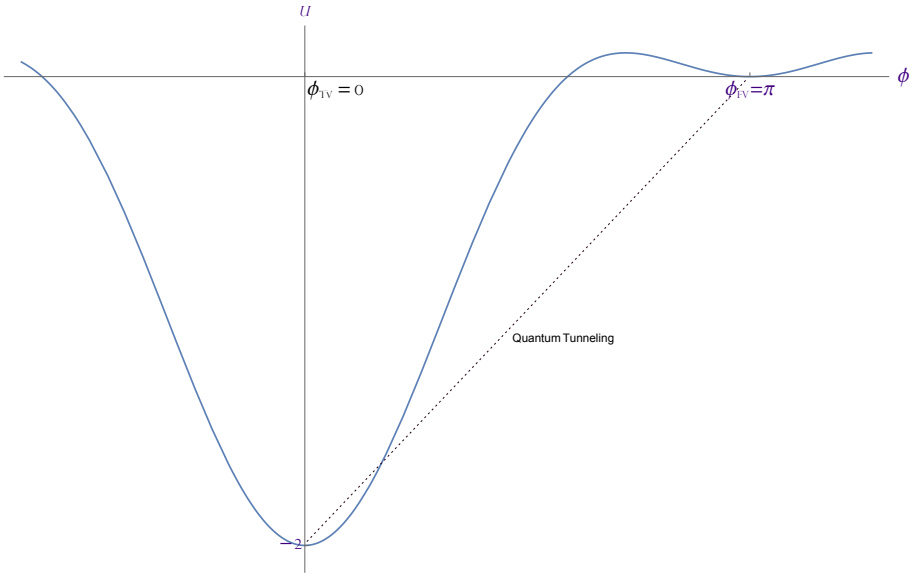

Figure 1.1: In classical field theory, the state for which $\phi = \phi_{\mathrm{TV}}$ is the unique classical state of lowest energy, and corresponds to the unique (true) vacuum state of the quantum theory of the field. As for $\phi = \phi_{\mathrm{FV}}$, however, the quantum and classical theories differ in that for the latter ϕ_{FV} is a stable classical equilibrium state, whereas for the quantum case ϕ_{FV} is rendered unstable by barrier penetration (i.e., quantum tunneling). For this reason, in quantum theory ϕ_{FV} is known as a false vacuum.

This simple (but not at all intuitive!) correspondence between cyclic imaginary time and inverse temperature come from the interface of two very successful theories: *Quantum Mechanics* (QM) and *Statistical mechanics* (SM).

$$\mathrm{e}^{-iHt/\hbar} \xrightarrow{t \to -i\tau} \mathrm{e}^{-H\tau/\hbar} \xrightarrow{\tau/\hbar \to \beta} \mathrm{e}^{-\beta H}$$

Figure 1.2: The correspondence between QM and SM. The leftmost object is the *time evolution operator* from QM and the rightmost object is the *density operator* from SM. The Euclidean time τ is cyclic with period β.

The thermal aspect of the bubble decay is represented by a periodicity imposed in the τ-coordinate, with period β. At low temperatures, the size of the bubble is small compared to β and thermal effects appear mostly through the form of the effective potential. [Lin83] On the other hand, at higher temperatures –provided the effective potential still has a potential barrier– the instanton solution becomes constant in the τ-direction. In between there is a cross-over region were instanton solutions become distorted; we see this transition in detail in Figures 1.3 & 3.3). When the temperature is very low (β is very large), the τ-direction is identical to the space directions, and we can expect that the solution has $O(D)$ symmetry (i.e., rotational symmetry of the full D-dimensional configuration). Such a solution (shown on the left of Figs 1.3 & 3.3) is said to describe *quantum tunnelling*. Conversely,

with increasing temperatures (decreasing β), the D-volume becomes "squeezed", and this reshapes the profile of the bubble solution (middle of Figs 1.3 & 3.3). In this case we say that both *quantum tunnelling* and *thermal fluctuations* play a role. Lastly, for very large T (even smaller β) the bubble profile becomes very squeezed, and we expect that the solution only respects $O(D-1)$ symmetry. [2] Such *classical thermal fluctuation* is shown on the right of Figs 1.3 & 3.3.

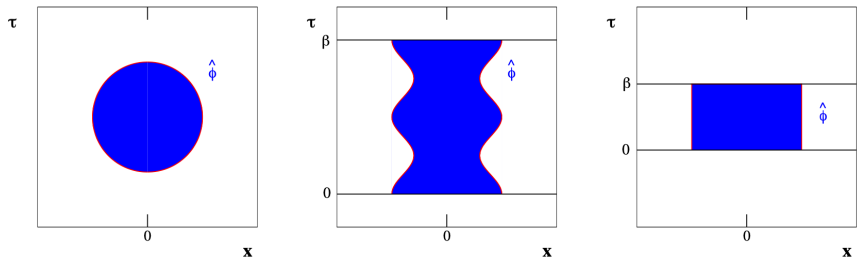

Figure 1.3: Transition from vacuum to thermal case. The figure shows the nontrivial bubble solution ϕ_b (here denoted $\hat{\phi}$) in various regimes: at zero (left), intermediate (middle), and high (right) temperatures. The image is taken from [LV16]; our numerical results shown in Fig 3.3 also show this transition.

We note that we shall not make any use whatsoever of the coefficient A in what follows; the interested reader is advised to consult the original work [CC77], where it is shown that

$$A = \left| \frac{\det' S_E''[\phi_b]}{\det S_E''[\phi_{FV}]} \right|^{-1/2} \left(\frac{S_E[\phi_b]}{2\pi} \right)^{N/2}. \tag{1.6}$$

Here ϕ_b is the ***bubble*** (or "***bounce***") solution to the equations of motion presented below (c.f. (1.7)), ϕ_{FV} is the value of the field in the false vacuum ($= \pi$), S_E'' denotes the second functional derivative of the Euclidean action (1.2), and lastly $\det'$ denotes omission of $N = n+1$ zero modes from the functional determinant of the operator in the vacuum case and $N = n$ zero modes for the thermal case.

[2] It is precisely because of this breaking of symmetry in the thermal case that we have endeavored to find a new numerical technique that solves the equation of motion of the caloron, since the usual shooting methods found in the literature are only applicable to the vacuum case (see full discussion on Chapter 2).

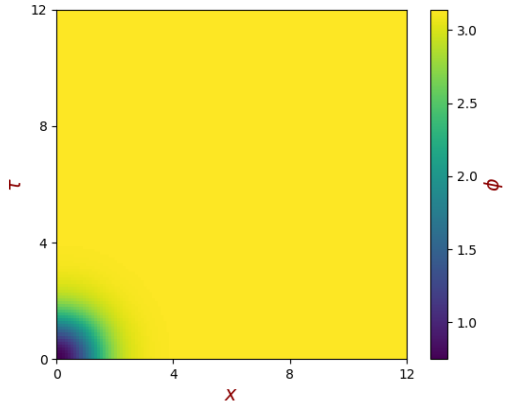

Figure 1.4: Initial data (one spatial dimension; vacuum case) given by (1.9), with $R = \varpi = 1$ and $\mathfrak{e} = 0$. Because of the symmetry assumptions on our bubble, there is no loss of generality in plotting just one quadrant ($x \geq 0, \tau \geq 0$). Note that away from the bubble, which is caused by quantum fluctuations, the false vaccuum persists (this is manifest in the boundary condition (1.8a) and $\lim_{\tau\to\pm\infty} \phi = \phi_{\mathrm{FV}} = \pi$, which holds true in the vacuum case.).

From variational principles, setting $\delta S_E = 0$ yields the *equation of motion*

$$\mathring{\nabla}^2\phi - \partial_\phi U = 0. \tag{1.7}$$

(From a quantum theory perspective, solutions to this equation of motion may be thought of as critical points of the action (1.2).) The term containing the gradient of the potential makes what would otherwise be a straightforward computation (a simple Laplacian) into an equation that is actually very difficult to tackle head on; we must thus resort to numerical methods. In light of the ineffectiveness of shooting methods when dealing with thermal fluctuations, we have developed from scratch a new relaxation scheme that has proven effective in both the vacuum and thermal cases. We shall present all our results in the following chapter, for up to three spatial dimensions. [3]

In the vacuum case, the field approaches the false vacuum value $\phi_{\mathrm{FV}} = \pi$ as $\tau \to \pm\infty$, while in the thermal case an initial thermal ensemble is represented by solutions that are periodic in τ with periodicity $\beta = 1/T$. Thus we may sum up the boundary conditions for the PDE (1.7) as [4]

$$\lim_{\|\vec{x}\|\to\infty} \phi = \phi_{\mathrm{FV}} = \pi \tag{1.8a}$$

$$\partial_{\vec{x}}\phi(\tau, \vec{x}_{\min}) = 0 \tag{1.8b}$$

$$\partial_\tau\phi(\tau_{\max}, \vec{x}) = \partial_\tau\phi(\tau_{\min}, \vec{x}) = 0. \tag{1.8c}$$

In our numerical implementations we shall use $\tau_{\min} = \vec{x}_{\min} = 0$ and $\vec{x}_{\max} = 12$, whilst $\tau_{\max}$ will be varied in order to consider a range of different temperatures. An approximate

[3] In all cases we assume rotational symmetry of the spatial coordinates; the full 3+1 asymmetric case will be considered in future developments which shall include gravity.

[4] A bit of thought should convince the reader that the last condition (1.8c) suits both the vacuum and thermal cases.

bubble solution (see Figure 1.4) we shall use later is given by [5]

$$\phi = \frac{\pi}{2}\left(2 + \tanh\frac{\mathfrak{d}-\mathfrak{R}}{\varpi} - \tanh\frac{\mathfrak{d}+\mathfrak{R}}{\varpi}\right), \tag{1.9}$$

where $\mathfrak{R}$ and ϖ are the radius and wall thickness (i.e., width), respectively, of the bubble. Moreover, we have $\mathfrak{d} = \sqrt{\mathfrak{a}\tau^2 + \mathfrak{b}\vec{x}^2}$, with the parameters $\mathfrak{a} = 1 - \mathfrak{e}^2$ and $\mathfrak{b} = 1 + \mathfrak{e}^2$ determined by the *ellipticity* $0 \leq \mathfrak{e} \leq 1$. In the case where $\mathfrak{e} = 0$ we shall refer to our field as the ***non-static instanton*** and for $\mathfrak{e} = 0.99$ (where the field is (nearly) independent of τ) we will call it the ***quasi-static instanton*** (these are the instances of most importance to our work). In the special case when the field is completely independent of τ (i.e., it is fully static, $\mathfrak{e} = 1$) the equation of motion (1.7) (in Cartesian coordinates) reduces to

$$\partial_{\vec{x}}^2\phi - \partial_\phi U = 0 \tag{1.10}$$

or, in one spatial dimension,

$$\frac{\mathrm{d}^2\phi}{\mathrm{d}x^2} - \partial_\phi U = 0. \tag{1.11}$$

Here we can easily find a closed-form solution: we have

$$\frac{\mathrm{d}\phi}{\mathrm{d}x} = \sqrt{2U}, \tag{1.12}$$

with the solution bouncing off the potential at $\phi_r = \arccos(1 - 2/\lambda^2)$. [6] The action (1.2) is then reduced to

$$S_E = 2\beta\int_{\phi_r}^{\phi_{\mathrm{FV}}}\sqrt{2U}\,\mathrm{d}\phi, \tag{1.13}$$

which can be obtained in closed-form,

$$S_E = 4\beta\left[\sqrt{\lambda^2-1} - \frac{1}{\lambda}\log\left(\sqrt{\lambda^2-1}+\lambda\right)\right]. \tag{1.14}$$

Finding such a nice, exact solution for (1.10) in higher spatial dimensions is not feasible, except for when the potential barrier is relatively large (large λ) in the so-called *thin-wall approximation*. ([AM20], [Col77]) Thus, in the general case, we must turn to numerical solutions; this is precisely what set out to accomplish in the remainder of this report.

[5] This approximation is the "guess" that we use as initial conditions for the relaxation technique we will present in the next chapter.

[6] $U(\phi_r) = \frac{1}{2}\lambda^2\left(1-\cos^2\phi_r\right) - \cos\phi_r - 1 = \frac{1}{2}\lambda^2\left[1 - \left(1-\frac{2}{\lambda^2}\right)^2\right] - \left(1-\frac{2}{\lambda^2}\right) - 1 = 0.$

CHAPTER 2

Numerical Techniques

A thorough comparison of the theory of bubble nucleation with the proposed table-top experiments in laboratory Bose-Einstein condensates ([Bra+19], [Fia+15]) requires precise numerical modeling. Such computations of bubble nucleation rates in cosmology are usually obtained using *shooting methods* (e.g., [AH92], [MR17]), an option that is viable thanks to the $O(D)$ symmetry enjoyed by the instanton solution in the vacuum case; under such symmetry assumptions the equation of motion can be reduced to an ODE that is easily solved using such methods. This symmetry, however, is not a feature present in the thermal case (as we clearly saw on Fig 1.3), and as a consequence we need to find an alternative approach.[AM20] We do, indeed, present in what follows a new numerical method that is valid for calculating nucleation exponents for both thermal and vacuum decay.

2.1 Basics of Relaxation Methods

The numerical method we employ in our work is a kind of *relaxation technique*. In the typical relaxation method we start with a guessed solution that satisfies the required boundary conditions and then is gradually modified to satisfy the difference equation within a given tolerance. The classic example is an elliptic PDE such as the Laplace equation (say, in two spatial dimensions),

$$D^2\varphi = \partial_x^2\varphi + \partial_y^2\varphi = 0 \tag{2.1}$$

which, using standard FDM techniques with equidistant spacing $\mathrm{h} = \Delta x = \Delta y$, is rewritten as

$$\frac{\varphi(x+\mathrm{h},y) - 2\varphi(x,y) + \varphi(x-\mathrm{h},y)}{\mathrm{h}^2} + \frac{\varphi(x,y+\mathrm{h}) - 2\varphi(x,y) + \varphi(x,y-\mathrm{h})}{\mathrm{h}^2} = 0. \tag{2.2}$$

Rearranging, and writing in standard FDM notation ($\varphi_{i,j} \equiv \varphi(x,y)$; $\varphi_{i\pm1,j} \equiv \varphi(x\pm\mathrm{h},y)$; $\varphi_{i,j\pm1} \equiv \varphi(x,y\pm\mathrm{h})$), we have

$$\varphi_{i,j} = \frac{\varphi_{i+1,j} + \varphi_{i-1,j} + \varphi_{i,j+1} + \varphi_{i,j-1}}{4}. \tag{2.3}$$

This shows the rather surprising property of the solution to Laplace's equation at any given point on the grid given as the average of the values at the four neighboring points. From (2.3) we may find an iterative scheme for finding solutions to the Laplace equation. As we alluded to above, we start with some initial ansatz/guess, [1] and then sweep across the grid updating

[1] The final solution should not depend on the initial values we guess, but the solution may converge more rapidly if we start with a good ansatz from the onset (i.e., if our guess is reasonably close to the final solution).

the value at each point (per (2.3)). This process is then repeated over and over until we converge to a solution. How do we know we have reached the desired solution? When the change from one iteration to the next is less than some specified tolerance, we declare the solution converged and break the loop. Of course, in theory we would like this change in solution to be zero, but such exact nature is not amenable to numerical computations. Instead we settle for a residual

$$r = \frac{\varphi_{i+1,j} + \varphi_{i-1,j} + \varphi_{i,j+1} + \varphi_{i,j-1}}{4} - \varphi_{i,j}$$

to reach a small-enough threshold $r \leq \epsilon$ at which the loop breaks. Intuitively, we may recast this as an evolution-boundary-value problem; start by turning (2.1) into a heat equation

$$\partial_t \varphi = \partial_x^2 \varphi + \partial_y^2 \varphi. \tag{2.4}$$

Then, writing $\varphi^n_{i,j}$ to denote the value of the function φ at the grid point $(x, y) = (i\mathrm{h}, j\mathrm{h})$ at time step $t = n$, the FDA of (2.4) is

$$\frac{\varphi^{n+1}_{i,j} - \varphi^n_{i,j}}{\Delta t} = \frac{\varphi^n_{i+1,j} + \varphi^n_{i-1,j} + \varphi^n_{i,j+1} + \varphi^n_{i,j-1} - 4\varphi^n_{i,j}}{\mathrm{h}^2}. \tag{2.5}$$

If we now choose (for simplicity) time stepping $\Delta t = \mathrm{h}^2/4$, we end up with

$$\varphi^{n+1}_{i,j} = \frac{\varphi^n_{i+1,j} + \varphi^n_{i-1,j} + \varphi^n_{i,j+1} + \varphi^n_{i,j-1}}{4}, \tag{2.6}$$

which is precisely the iteration described by (2.3), though now with a "time" label. In other words, we can think of our relaxation ploy as a time evolution scheme that searches for a *steady-state* configuration that satisfies Laplace's equation.

As to how exactly we perform the sweep across the grid, there are quite a few options to work with. Our implementation will be the so-called *Jacobi method*, in which we compute all the new values for φ at all grid points before moving on to the next iteration. Admittedly, a method such as the *Gauss-Seidel* relaxation –in which we immediately use the updated values to compute the new values at the neighboring points– is much faster than using Jacobi, but the latter suffices for our needs in the problem at hand.

2.2 Back to our Model. Weak Relaxation.

By using $\tau = it$ instead of coordinate time t, our equation of motion (1.7) is treated as a boundary value problem (BVP) as opposed to an initial value problem (IVP). In such setting, a relaxation scheme is quite appropriate; thus we proceed by introducing an extra "time" dimension s and an auxiliary scalar $\Phi(s, \tau, x)$. At this point we may naïvely attempt to solve (1.7) by using a relaxation method as discussed above:

$$\frac{\mathrm{d}\Phi}{\mathrm{d}s} = \mathcal{O}\mathcal{F}, \tag{2.7a}$$

where $\mathcal{F}[\Phi] \equiv -S'_E[\Phi]$ is the *residual*

$$\mathcal{F} = \mathring{\nabla}^2\Phi - \partial_\Phi U, \tag{2.8}$$

and the operator $\mathcal{O}$ is introduced to ensure that the scheme converges to the desired solution ϕ_b (i.e., to ensure that $\lim_{s\to\infty}\Phi(s,\tau,x) = \phi_b(\tau,x)$). The simplest such operator is the identity operator, which yields

$$\frac{\mathrm{d}\Phi}{\mathrm{d}s} = \mathcal{F}. \tag{2.7b}$$

We now proceed using one spatial dimension, writing $\Phi^n_{i,j}$ for the value of the field Φ at the grid point $(\tau,x) = (i\mathrm{h}, j\mathrm{h})$ at the time step $s = n$. Discretising (2.7b),

$$\frac{\Phi^{n+1}_{i,j} - \Phi^n_{i,j}}{\Delta s} = \frac{\Phi^n_{i+1,j} + \Phi^n_{i-1,j} + \Phi^n_{i,j+1} + \Phi^n_{i,j-1} - 4\Phi^n_{i,j}}{\mathrm{h}^2} - \frac{\lambda^2}{2}\sin\left(2\Phi^n_{i,j}\right) + \sin\Phi^n_{i,j} \tag{2.9a}$$

or, rearranging,

$$\Phi^{n+1}_{i,j} = \varsigma\left[\Phi^n_{i+1,j} + \Phi^n_{i-1,j} + \Phi^n_{i,j+1} + \Phi^n_{i,j-1}\right] + \Phi^n_{i,j}\left[1 - 4\varsigma\right] - \Delta s\left[\frac{\lambda^2}{2}\sin\left(2\Phi^n_{i,j}\right) + \sin\Phi^n_{i,j}\right] \tag{2.9b}$$

with

$$\varsigma \equiv \frac{\Delta s}{\mathrm{h}^2}. \tag{2.10}$$

Thus, Equation (2.9b) yields an expression for Φ at the the next "s" time step in terms of the current "s" time step; since this is an *explicit* scheme, we need to be mindful of the Courant-Friedrichs-Lewy (CFL) condition (we have found that $\varsigma \lesssim 1/2$ works). However, there is a problem with this particular relaxation method: regardless of which value we pick for ς, the algorithm does not remain stable for long (this has to do with the spectrum of $\mathcal{F}$; more on this shortly). Hence, after not many interations, (2.9b) will always relax to a vacuum state, be it the false or the true vacuum (whether we end up with ϕ_{FV} or ϕ_{TV} depends heavily on the height of the potential barrier, and hence on the parameter λ).

2.3 Back to our Model. Strong Relaxation.

The procedure presented in the previous two sections outlines the methodology we are to employ in our work. However, moving forward there are a couple of changes that need to be made, as evident by the instability of (2.9b). Let us examine the response of the field near the solution Φ_b under the effect of a slight perturbation $\delta\Phi$:

$$\frac{\mathrm{d}\Phi}{\mathrm{d}s} = \frac{\mathrm{d}}{\mathrm{d}s}\left(\Phi_b + \delta\Phi\right) = \underbrace{\frac{\mathrm{d}\Phi_b}{\mathrm{d}s}}_{=0} + \frac{\mathrm{d}(\delta\Phi)}{\mathrm{d}s} = \frac{\mathrm{d}(\delta\Phi)}{\mathrm{d}s}. \tag{2.11}$$

Hence the behavior of the system close to the bubble solution Φ_b is governed by a second-order operator $\mathcal{F}'[\Phi_b] \equiv \delta\mathcal{F}[\Phi_b]/\delta\Phi$ ($\equiv -S''_E[\Phi_b]$), which is given from (2.7a) by

$$\frac{\mathrm{d}(\delta\Phi)}{\mathrm{d}s} = \mathcal{O}\mathcal{F}'\delta\Phi. \tag{2.12}$$

Now, choosing $\mathcal{O}$ in such a way that $\mathcal{O}\mathcal{F}'$ has a positive spectrum leads to convergence in a neighborhood of the solution Φ_b. However note that, since the operator $\mathcal{F}'$ has negative

eigenvalues, we are barred from choosing $\mathcal{O}$ to be a multiple of the identity (as we did earlier). Two obvious choices that fulfill the positive spectrum requirement of $\mathcal{O}\mathcal{F}'$ are $\mathcal{O} = (\mathcal{F}')^{-1}$ and $\mathcal{O} = (\mathcal{F}')^\dagger$. The former gives convergence, but it requires a matrix inversion step that may itself be problematic due to small eigenvalues of $\mathcal{F}'$. That leaves $(\mathcal{F}')^\dagger$ as the best choice, which we denote by $\Delta^\dagger$; its action on $\mathcal{F}$ is given by

$$\Delta^\dagger \mathcal{F} \equiv (\mathcal{F}')^\dagger \mathcal{F} = -\mathring{\nabla}^2 \mathcal{F} + \partial_\Phi^2 U \mathcal{F}. \tag{2.13}$$

We plug this back into (2.7a):

$$\frac{\mathrm{d}\Phi}{\mathrm{d}s} = \Delta^\dagger \mathcal{F}. \tag{2.14a}$$

However, we are not entirely out of the woods just yet; as the von Neumann stability analysis that we will perform shortly reveals, the choice $\mathcal{O} = \Delta^\dagger$ requires a very small numerical relaxation time step ($\Delta s \sim O(\mathrm{h}^4)$; c.f.,Proposition 2.3.1). How do we get around this problem? It turns out that recasting (2.14a) as a second-order, damped-oscillator equation in relaxation time,

$$\frac{\mathrm{d}^2\Phi}{\mathrm{d}s^2} + k\frac{\mathrm{d}\Phi}{\mathrm{d}s} = \Delta^\dagger \mathcal{F} \tag{2.14b}$$

provides a stable algorithm that only requires $\Delta s \sim O(\mathrm{h}^2)$ (c.f.,Proposition 2.3.2) for stability (provided we use central differencing for the relaxation time derivatives). We now comment on the damping coefficient k: the convergence of (2.14b) is related to the eigenvalue spectrum of $\mathcal{F}'[\phi]$. If we consider a single mode with eigenvalue η, then the amplitude $\delta\phi_\eta$ of the mode decays exponentially,

$$\delta\phi_\eta \propto e^{-ks+\sqrt{k^2-|\eta|^2}s}. \tag{2.15}$$

For large values of $|\eta|$, the convergence is determined by k, and for small $|\eta|$ by $|\eta|^2/(2k)$. Thus, the optimal value of k would be $k \approx |\eta_{\min}|$, where $\eta_{\min}$ is the eigenvalue with smallest modulus. In practice we ended up only using $k = 1$ in our code.

Finite-differencing (2.14b), we get

$$\boxed{\Phi_{i,j}^{n+1} = \frac{1}{1+\frac{k}{2}\Delta s}\left\{2\Phi_{i,j}^n - \Phi_{i,j}^{n-1}\left[1-\frac{k}{2}\Delta s\right] + \Delta^\dagger\mathcal{F}(\Phi_{i,j}^n)\Delta s^2\right\}} \tag{2.16}$$

This algorithm has proven to be quite robust in all cases tested. Note that the $\Phi_{i,j}^{n-1}$ term mandates that we know the value of the field Φ at the $s = -1$ step; we set $\Phi_{i,j}^{-1} = \Phi_{i,j}^0$, since the solutions are damped oscillations and this boundary condition fixes the phase of the oscillation.

von Neumann Analysis

The von Neumann stability analysis of a time-dependent PDE is based on the assumptions that the PDE has constant coefficients (or at the very least the coefficients vary so slowly as to be considered constant), and that the PDE is subject to periodic boundary conditions. Despite the latter, the analysis actually proves useful even in cases where the boundary

conditions are nonperiodic, so we may apply it in all our cases of interest (static, quasi-static, thermal, vacuum). Throughout this subsection we will suppress the spatial dimension for clarity, since the expressions dependent on τ are identical to the expressions dependent on x; i.e., a stability analysis on $\Phi(s,\tau)$ is trivially extended to $\Phi(s,\tau,x)$. To that end we shall write Φ_i^n in place of $\Phi_{i,j}^n$.

The analysis is usually written in terms of the roundoff error

$$\varepsilon_i^n \equiv \tilde{\Phi}_i^n - \Phi_i^n, \tag{2.17}$$

where Φ_i^n is our numerical solution and $\tilde{\Phi}_i^n$ is the finite-precision solution. Then for periodic boundary conditions over some domain $[0, L]$, the error can be represented as a discrete Fourier series

$$\varepsilon(s,\tau) = \sum_m A_m e^{\iota\omega_m\tau}, \tag{2.18}$$

where $\omega_m = (2\pi m)/L$ is the wave number. (Note also that we are using ι to denote the imaginary number $\sqrt{-1}$ to avoid any confusions with the index i.) In our grid then (2.18) takes the form

$$\varepsilon_i^n = \sum_m A_m^n e^{\iota\omega_m\tau_i}, \tag{2.19}$$

where A_m^n is the value of the Fourier coefficient A_m at $n\Delta s$, i.e., at the "time step" n. Moving forward we shall focus our analysis only on one term of the full series, since (by the linearity of our FDAs) it is enough to consider the growth of error of a single Fourier harmonic term. Moreover, instead of writing everything in terms of the error ε, we shall instead write out the analysis in terms of the actual numerical solution $\Phi(s,\tau)$. Hence, from now on we will replace (2.19) with

$$\Phi_i^n = A^n e^{\iota\omega\tau_i}. \tag{2.20}$$

The *von Neumann stability criterium* states that the FDA of the PDE being analyzed is stable, provided that

$$|\alpha| \leq 1, \tag{2.21}$$

where α is the *amplification factor*

$$\alpha \equiv \frac{A^{n+1}}{A^n}. \tag{2.22}$$

We are now ready to prove the following stability claims we made earlier:

Proposition 2.3.1. *The numerical relaxation time step Δs of the FDA (2.14a) is of order $\sim O(\mathrm{h}^4)$.*

Proposition 2.3.2. *The numerical relaxation time step Δs of the FDA (2.14b) is of order $\sim O(\mathrm{h}^2)$.*

Note what the propositions actually state; we are not doing a full stability analysis, but rather searching for some guidance to determine what Δs steps might work with the code. A more thorough analysis is outside our scope. To that end in the proofs we shall use a truncated $\Delta^\dagger\mathcal{F}$ term; expanding (2.13), we have

$$\Delta^\dagger\mathcal{F} = -\partial_\tau^4\Phi - \partial_x^4\Phi + \Upsilon(U), \tag{2.23a}$$

where $\Upsilon(U)$ is an expression containing gradients of the potential that we exclude from our stability analysis. Moreover, the gradient $-\partial_x^4\Phi$ is also excluded because of the omission

of the spatial coordinate (we discussed the grounds for doing this at the beginning of this subsection). Hence we shall work instead with

$$\Delta^{\dagger}\mathcal{F} = -\partial_{\tau}^{4}\Phi. \tag{2.23b}$$

Proof of Proposition 2.3.1. Equation (2.14a) is now written as

$$\frac{\mathrm{d}\Phi}{\mathrm{d}s} = -\partial_{\tau}^{4}\Phi, \tag{2.24}$$

which FDA is

$$\frac{\Phi_i^{n+1} - \Phi_i^{n-1}}{2\Delta s} = -\frac{\Phi_{i+2}^{n} - 4\Phi_{i+1}^{n} + 6\Phi_i^{n} - 4\Phi_{i-1}^{n} + \Phi_{i-2}^{n}}{\mathrm{h}^4}. \tag{2.25}$$

Writing $\Sigma \equiv \Delta s/\mathrm{h}^4$ and rearranging, we get

$$\Phi_i^{n+1} = -2\Sigma\left\{\Phi_{i+2}^{n} - 4\Phi_{i+1}^{n} + 6\Phi_i^{n} - 4\Phi_{i-1}^{n} + \Phi_{i-2}^{n}\right\} + \Phi_i^{n-1}, \tag{2.26}$$

and then using (2.20),

$$\begin{aligned} A^{n+1}e^{\imath\omega\tau_i} = -2\Sigma\left\{A^{n}e^{\imath\omega\tau_{i+2}} - 4A^{n}e^{\imath\omega\tau_{i+1}} + 6A^{n}e^{\imath\omega\tau_i} - 4A^{n}e^{\imath\omega\tau_{i-1}} + A^{n}e^{\imath\omega\tau_{i-2}}\right\} \\ + A^{n-1}e^{\imath\omega\tau_i}. \end{aligned} \tag{2.27}$$

We now divide both sides by $A^n e^{\imath\omega\tau_i}$, noting that $e^{\imath\omega\tau_{i\pm1}} = e^{\imath\omega\tau_i}e^{\pm\imath\omega\mathrm{h}}$ and that $A^{n-1}/A^n = A^n/A^{n+1} = \alpha^{-1}$:

$$\alpha = -2\Sigma\left\{e^{2\imath\omega\mathrm{h}} - 4e^{\imath\omega\mathrm{h}} + 6 - 4e^{-\imath\omega\mathrm{h}} + e^{-2\imath\omega\mathrm{h}}\right\} + \frac{1}{\alpha}. \tag{2.28}$$

Then we multiply through by α, and use the identities

$$\cos\varphi = \frac{e^{\imath\varphi} + e^{-\imath\varphi}}{2} \quad \text{and} \quad \cos(2\varphi) = 2\cos^2\varphi - 1, \tag{2.29}$$

to get

$$\begin{aligned} \alpha^2 &= -2\alpha\Sigma\left\{\left(e^{2\imath\omega\mathrm{h}} + e^{-2\imath\omega\mathrm{h}}\right) - 4\left(e^{\imath\omega\mathrm{h}} + e^{-\imath\omega\mathrm{h}}\right) + 6\right\} + 1 \\ &= -2\alpha\Sigma\left\{2\cos(2\omega\mathrm{h}) - 8\cos(\omega\mathrm{h}) + 6\right\} + 1 \\ &= -4\alpha\Sigma\left\{2\cos^2(\omega\mathrm{h}) - 4\cos(\omega\mathrm{h}) + 2\right\} + 1 \\ &= -8\alpha\Sigma\left\{\cos^2(\omega\mathrm{h}) - 2\cos(\omega\mathrm{h}) + 1\right\} + 1 \\ &= -8\alpha\Sigma\left[\cos(\omega\mathrm{h}) - 1\right]^2 + 1. \end{aligned} \tag{2.30}$$

The sinusoidal term comes up again in our analysis; let us denote it as

$$\Theta \equiv \left[\cos(\omega\mathrm{h}) - 1\right]^2. \tag{2.31}$$

Thus we have an equation quadratic in α,

$$\alpha^2 + 8\Sigma\Theta\alpha - 1 = 0. \tag{2.32}$$

Our goal is not to solve this equation, but rather use the von Neumann stability criterion (2.21) to find the order of Δs. Plugging in either 1 or -1 for α in (2.32) does not help since the whole expression vanishes. Let us instead use, say $\alpha = 9/10$. Then

$$\frac{81}{100} + \frac{720}{100}\Sigma\Theta = 1 \implies \Delta s = \frac{19\mathrm{h}^4}{720\Theta}.$$

This shows that $\Delta s \sim O(\mathrm{h}^4)$, as we set out to prove. ■

Proof of Proposition 2.3.2. Now we check for the stability of the damped-oscillator equation (2.14b):

$$\frac{\mathrm{d}^2\Phi}{\mathrm{d}s^2} + k\frac{\mathrm{d}\Phi}{\mathrm{d}s} = -\partial_\tau^4\Phi, \tag{2.33}$$

which FDA is

$$\begin{aligned}&\frac{\Phi_i^{n+1} - 2\Phi_i^n + \Phi_i^{n-1}}{\Delta s^2} + k\frac{\Phi_i^{n+1} - \Phi_i^{n-1}}{2\Delta s}\\ &= -\frac{\Phi_{i+2}^n - 4\Phi_{i+1}^n + 6\Phi_i^n - 4\Phi_{i-1}^n + \Phi_{i-2}^n}{\mathrm{h}^4}.\end{aligned} \tag{2.34}$$

We can rewrite this (c.f., (2.16)) as

$$\begin{aligned}\Phi_i^{n+1} &= \frac{1}{1+\frac{k}{2}\Delta s}\{2\Phi_i^n - \Phi_i^{n-1}\left[1 - \frac{k}{2}\Delta s\right]\\ &\quad - \left(\Phi_{i+2}^n - 4\Phi_{i+1}^n + 6\Phi_i^n - 4\Phi_{i-1}^n + \Phi_{i-2}^n\right)\varsigma^2\}\\ &= \frac{1}{1+\frac{k}{2}\Delta s}\{\Phi_i^n\left[2 - 6\varsigma^2\right] - \Phi_i^{n-1}\left[1 - \frac{k}{2}\Delta s\right]\\ &\quad + \left(4(\Phi_{i+1}^n + \Phi_{i-1}^n) - \Phi_{i+2}^n - \Phi_{i-2}^n\right)\varsigma^2\},\end{aligned} \tag{2.35}$$

where ς is given by (2.10). As before we write everything as Fourier harmonic terms,

$$\begin{aligned}A^{n+1}e^{\imath\omega\tau_i} &= \frac{1}{1+\frac{k}{2}\Delta s}\{A^n e^{\imath\omega\tau_i}\left[2 - 6\varsigma^2\right] - A^{n-1}e^{\imath\omega\tau_i}\left[1 - \frac{k}{2}\Delta s\right]\\ &\quad + \left(4(A^n e^{\imath\omega\tau_{i+1}} + A^n e^{\imath\omega\tau_{i-1}}) - A^n e^{\imath\omega\tau_{i+2}} - A^n e^{\imath\omega\tau_{i-2}}\right)\varsigma^2\}\end{aligned} \tag{2.36}$$

which, dividing by $A^n e^{\imath\omega\tau_i}$, becomes

$$\begin{aligned}\alpha &= \frac{1}{1+\frac{k}{2}\Delta s}\{2 - 6\varsigma^2 - \frac{1}{\alpha}\left[1 - \frac{k}{2}\Delta s\right]\\ &\quad + \left(4(e^{\imath\omega\mathrm{h}} + e^{-\imath\omega\mathrm{h}}) - (e^{2\imath\omega\mathrm{h}} + e^{-2\imath\omega\mathrm{h}})\right)\varsigma^2\}.\end{aligned} \tag{2.37}$$

Mutiplying through by α and using (2.29) and (2.31), we get the following quadratic equation after rearranging terms:

$$\alpha^2\left(1 + \frac{k}{2}\Delta s\right) - 2\left(1 - 2\varsigma^2\Theta\right)\alpha + 1 - \frac{k}{2}\Delta s = 0. \tag{2.38}$$

Letting $\alpha = 1$ makes the whole expression vanish; let us instead try $\alpha = -1$:

$$\left(1 + \frac{k}{2}\Delta s\right) + 2\left(1 - 2\varsigma^2\Theta\right) + 1 - \frac{k}{2}\Delta s = 0 \quad \Longrightarrow \quad \Delta s = \frac{\mathrm{h}^2}{\sqrt{\Theta}}.$$

Thus we have shown that $\Delta s \sim O(\mathrm{h}^2)$, which makes (2.14b) the more desirable algorithm. ■

CHAPTER 3

Results & Conclusions

We now show all the relevant numerical results obtained from the equation of motion of our instanton. Let us start with the the Euclidean action of the field (1.2). In the 1+1D case, we have

$$S_E = \int \left\{ \frac{1}{2} \left[(\partial_\tau \Phi)^2 + (\partial_x \Phi)^2 \right] + U \right\} \mathrm{d}\tau \, \mathrm{d}x. \tag{3.1a}$$

To numerically evaluate this double integral we implement a 2D composite Simpson method (see § A.1) which, for uniform grid spacing h, is given by the *Frobenius inner product* [1]

$$S_E \approx \frac{\mathrm{h}^2}{9} \boldsymbol{S} \otimes_F \mathcal{L} \equiv \frac{\mathrm{h}^2}{9} \sum_{i=\tau_{\min}}^{\tau_{\max}} \sum_{j=x_{\min}}^{x_{\max}} \boldsymbol{S}_{ij} \, \mathcal{L}_{ij}. \tag{3.2}$$

Here $\boldsymbol{S}$ is the Simpson coefficient matrix (c.f., (A.20)) and $\mathcal{L}_{ij}$ is the finite-difference approximation (FDA) of the Lagrangian

$$\mathcal{L} = \frac{1}{2} \left[(\partial_\tau \Phi)^2 + (\partial_x \Phi)^2 \right] + U. \tag{3.3}$$

The extension of this calculation to two and three spatial dimensions (with $O(D-1)$ symmetry) is straightforward. In these cases the action (1.2), rewritten in spherical coordinates, takes the form

$$^{2D}S_E = 2\pi \int \left\{ \frac{1}{2} \left[(\partial_\tau \Phi)^2 + (\partial_r \Phi)^2 \right] + U \right\} r \, \mathrm{d}\tau \, \mathrm{d}r \tag{3.1b}$$

$$^{3D}S_E = 4\pi \int \left\{ \frac{1}{2} \left[(\partial_\tau \Phi)^2 + (\partial_r \Phi)^2 \right] + U \right\} r^2 \, \mathrm{d}\tau \, \mathrm{d}r, \tag{3.1c}$$

where $r \equiv \sqrt{\sum_i (x^i)^2}$ is the radial coordinate. The only other consideration that we must take into account is how the gradients $\hat{\nabla}_a \Phi$ change when written in the new coordinates. In such cases the residual (2.8) is written as

$$^{2D}\mathcal{F}(\Phi) = \partial_\tau^2 \Phi + \partial_r^2 \Phi + \frac{1}{r} \partial_r \Phi - \partial_\Phi U \tag{3.4a}$$

$$^{3D}\mathcal{F}(\Phi) = \partial_\tau^2 \Phi + \partial_r^2 \Phi + \frac{2}{r} \partial_r \Phi - \partial_\Phi U. \tag{3.4b}$$

[1] Of course, since in our code we are using only one quadrant of the whole grid, (3.2) must be multiplied by 4 in order to get the full action.

To work around the coordinate singularity at $r = 0$ we Taylor-expand Φ in a neighborhood of $r = 0$,

$$\begin{aligned}\Phi(s,\tau,r) &= \Phi(s,\tau,0) + (r-0)\cancelto{0}{\partial_r\Phi(s,\tau,0)} + \frac{(r-0)^2}{2!}\partial_r^2\Phi(s,\tau,0) + O(r^3)\\ &\approx \Phi(s,\tau,0) + \frac{r^2}{2}\partial_r^2\Phi(s,\tau,0),\end{aligned} \tag{3.5}$$

where $\partial_r\Phi(s,\tau,0)$ vanished because of the boundary condition (1.8b). Taking the r-derivative of this expression, [2]

$$\begin{aligned}\partial_r\Phi(s,\tau,r) &\approx \partial_r\left(\Phi(s,\tau,0) + \frac{r^2}{2}\partial_r^2\Phi(s,\tau,0)\right)\\ &= \cancelto{0}{\partial_r[\Phi(s,\tau,0)]} + r\,\partial_r^2\Phi(s,\tau,0) + \frac{r^2}{2}\cancelto{0}{\partial_r[\partial_r^2\Phi(s,\tau,0)]}\\ &= r\,\partial_r^2\Phi(s,\tau,0).\end{aligned} \tag{3.6}$$

Hence, in a neighborhood of $r = 0$, we have

$$\frac{1}{r}\partial_r\Phi(s,\tau,r) \approx \partial_r^2\Phi(s,\tau,0).$$

Thus, we rewrite (3.4) as

$${}^{2D}\mathcal{F}(\Phi) = \begin{cases}\partial_\tau^2\Phi + 2\partial_r^2\Phi - \partial_\Phi U & \text{if } r = 0,\\ \partial_\tau^2\Phi + \partial_r^2\Phi + \frac{1}{r}\partial_r\Phi - \partial_\Phi U & \text{otherwise;}\end{cases} \tag{3.4c}$$

$${}^{3D}\mathcal{F}(\Phi) = \begin{cases}\partial_\tau^2\Phi + 3\partial_r^2\Phi - \partial_\Phi U & \text{if } r = 0,\\ \partial_\tau^2\Phi + \partial_r^2\Phi + \frac{2}{r}\partial_r\Phi - \partial_\Phi U & \text{otherwise.}\end{cases} \tag{3.4d}$$

Figure 3.1 shows the relation between action and temperature for both non-static and quasi-static initial conditions, in all three dimensional cases. Two curious observations are *a)* that we did not find any evidence for a non-static solution with higher action than the quasi-static solution, and *b)* that the critical temperature at which the transition takes place decreases with increasing dimensions.

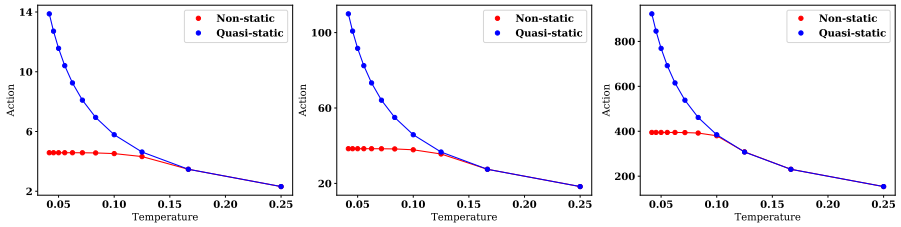

Figure 3.1: The plots show the dependence of the Euclidean action on temperature for non-static and quasi-static instantons. From left to right we show one, two, and three spatial dimensions. In all cases $\lambda = 1.2$.

[2] Do note the subtlety in notation; $\partial_r\Phi(s,\tau,0)$ vanished because of the boundary condition (1.8b), whereas $\partial_r[\Phi(s,\tau,0)]$ vanishes because we are taking the r-derivative of a constant expression ($\Phi(s,\tau,0)$).

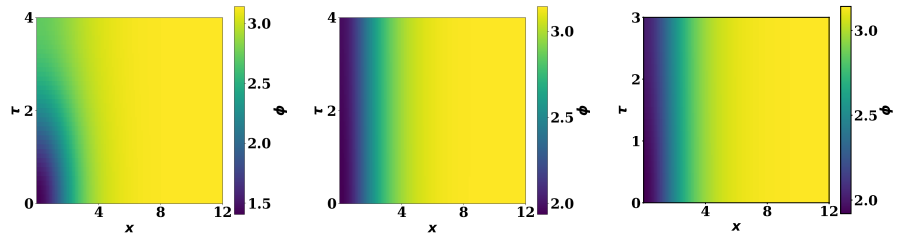

Figure 3.2: At $T = 0.125$, the non-static instanton (left) becomes distorted in the imaginary time direction. In the middle figure we show the quasi-static instanton at that very same temperature. Pushing the non-static field to a higher temperature $T = 0.17$ breaks its $O(2)$ symmetry even further and its profile (right) becomes identical to the quasi-static field shown in the middle.

Let us inspect the situation closer near the critical transitional temperature…Consider, for instance, the 1+1D case (left canvas on Fig 3.1). At around $T = 0.125$ the non-static instanton is becoming distorted and is starting to look a lot like the quasi-static bubble. If we push the temperature just a bit further to, say, $T = 0.17$, the profiles of the non-static and quasi-static fields become indistinguishable (see Fig 3.2). Focusing strictly on the non-static instanton, we see this transition from vacuum to thermal fluctuations on Figure 3.3 (compare this figure to Fig 1.3).

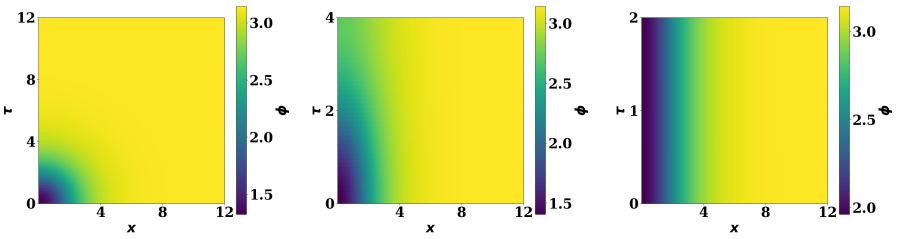

Figure 3.3: Transition from vacuum to thermal case of the non-static ($\mathfrak{e} = 0$) instanton, and the breaking of its $O(2)$ symmetry (one spatial dimension). The figure shows minimum [$T \approx 0.04$] (left), medium [$T = 0.125$] (middle), and high [$T = 0.25$] (right) temperatures. We can see how the rotational symmetry of the bubble is broken as temperatures increase. In all cases $\lambda = 1.2$.

The action also shows a dependence on the height of the potential barrier, which is given by the parameter λ; we show this relation on Fig 3.4. We can quantify this relation through a least squares fitting; let us consider the case with quasi-static initial conditions. From our data (see Table 3.1) we can infer an ansatz $S_E \approx \alpha/(2T)$ for some constant α; let us instead absorb this factor of 2 in α and proceed with a fitting for the ansatz

$$S_E = \frac{\alpha}{T}. \tag{3.7}$$

	T	S_E	
x_0	0.0416667	13.8767	y_0
x_1	0.0454545	12.7177	y_1
x_2	0.05	11.567	y_2
x_3	0.0555556	10.4083	y_3
x_4	0.0625	9.25161	y_4
x_5	0.0714286	8.09933	y_5
x_6	0.0833333	8.09933	y_6
x_7	0.1	5.78424	y_7
x_8	0.125	4.62776	y_8
x_9	0.166667	3.47151	y_9
x_{10}	0.25	2.31488	y_{10}

Table 3.1: Relation between action and temperature for the quasi-static, 1+1D instanton.

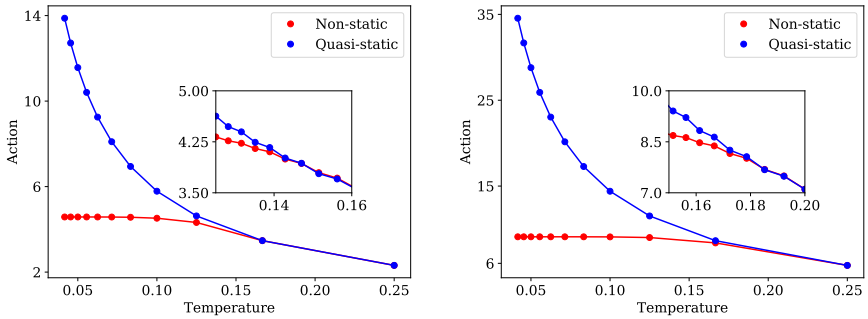

Figure 3.4: The plots show the dependence of the Euclidean action on temperature for non-static and quasi-static instantons with different potential barrier heights (left: $\lambda = 1.2$; right: $\lambda = 1.4$).

Then, via a least-squares fitting (§ A.2), α is furnished from

$$\alpha = \frac{\sum_i \frac{y_i}{x_i}}{\sum_i x_i^{-2}}. \tag{3.8}$$

Figure 3.5 shows the fitting of α with the action of quasi-static instanton for all three dimensional cases, as well as the (surprisingly linear!) relation between α and the potential barrier parameter λ.

This brings us to the conclusion of our study. We have investigated the cross-over regime of bubble nucleation, where the tunnelling instantons that dominate the nucleation rate lose one degree of symmetry in the presence of non-zero temperatures. The numerical results were obtained using a new relaxation technique that is amenable to both vacuum and thermal ensembles, and we found that the distorted instantons merge smoothly into quasi-static instantons.

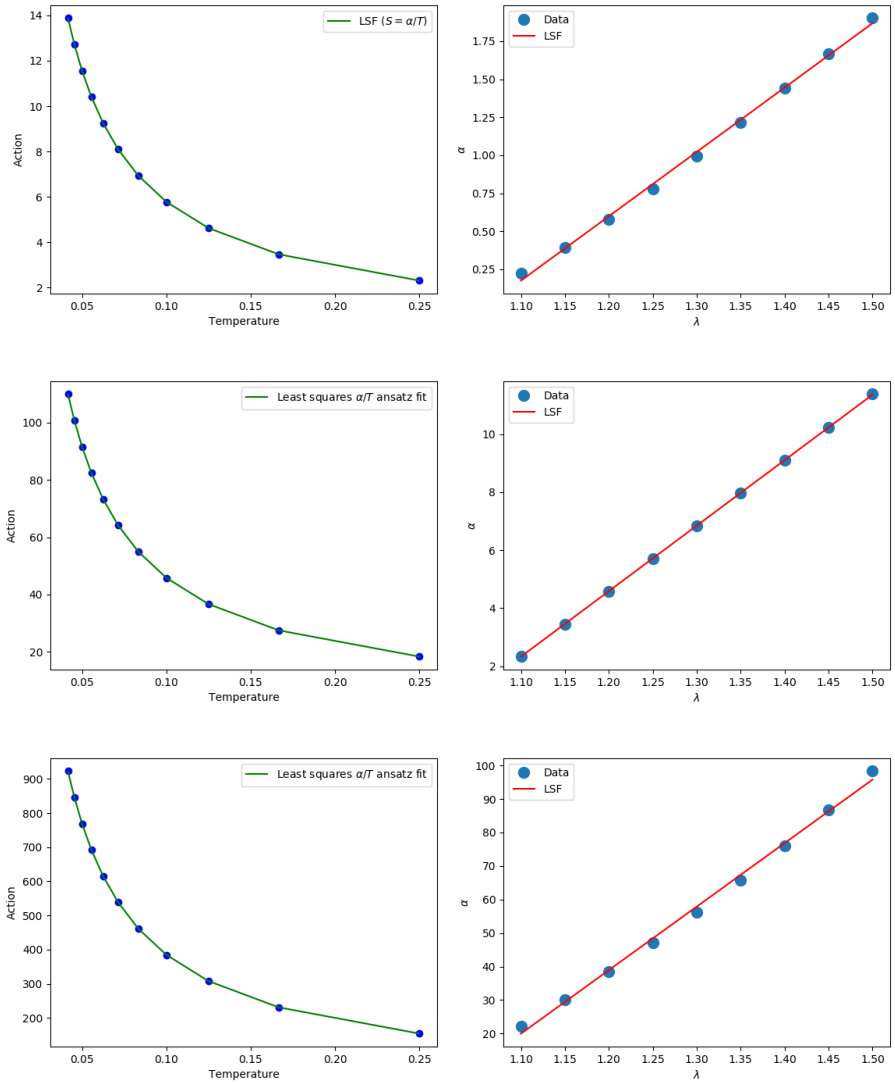

Figure 3.5: Least-squares fitting for $S_E = \alpha / T$ (left). This value of α is saved for different values of λ, from which we discover a surprisingly linear relation between α and λ (right), and consequently shows λ's dependence on T. The figure shows results for one (top), two (middle), and three (bottom) spatial dimensions.

Appendices

APPENDIX A

Numerical Methods

In this appendix we fill in some detail of a handful of numerical methods that we used in this report (the presentation is terse; it merely serves as a brief under-the-hood peek). Partial differential equations (PDE's) cannot be implemented using a computer in such raw form, as the computer would not be able to understand what the concept of a derivative is; hence we must settle for just an *approximation* of these derivatives. In typical Finite Difference Methods (FDM) fashion, we present some field/function and a discrete lattice, and then we evaluate certain combinations of values of this field at each lattice node in order to approximate its derivatives. (This approximation is usually referred to as the Finite-Difference Approximation, or FDA.)

Let Φ be a field, sufficiently smooth so that it admits a Taylor series expansion about some point x. Then we write

$$\Phi(x+\Delta x) = \sum_{n=0}^{\infty} \partial_x^n \Phi(x) \frac{\Delta x^n}{n!} = \Phi(x) + \partial_x \Phi \Delta x + \partial_x^2 \Phi \frac{\Delta x^2}{2} + \partial_x^3 \Phi \frac{\Delta x^3}{6} + \dots \tag{A.1}$$

or

$$\Phi(x-\Delta x) = \sum_{n=0}^{\infty} \partial_x^n \Phi(x) \frac{(-1)^n \Delta x^n}{n!} = \Phi(x) - \partial_x \Phi \Delta x + \partial_x^2 \Phi \frac{\Delta x^2}{2} - \partial_x^3 \Phi \frac{\Delta x^3}{6} + \dots \tag{A.2}$$

Note that from either (A.1) or (A.2) we can get an expression for the first derivative of Φ, by isolating the second term on the RHS and then dividing by Δx. For instance, for (A.1),

$$\partial_x \Phi = \frac{\Phi(x+\Delta x) - \Phi(x)}{\Delta x} - \partial_x^2 \Phi \frac{\Delta x}{2} - \partial_x^3 \Phi \frac{\Delta x^2}{6} - \dots \tag{A.3}$$

Now the green part of equation (A.3) must be truncated at some point, since the computer is not capable of dealing with infinite sums; whence we write

$$\partial_x \Phi = \frac{\Phi(x+\Delta x) - \Phi(x)}{\Delta x} + O(\Delta x). \tag{A.4}$$

Similarly, from (A.2),

$$\partial_x \Phi = \frac{\Phi(x) - \Phi(x-\Delta x)}{\Delta x} + O(\Delta x). \tag{A.5}$$

Moreover, substracting (A.2) from (A.1), we have

$$\partial_x \Phi = \frac{\Phi(x+\Delta x) - \Phi(x-\Delta x)}{2\Delta x} + O(\Delta x). \tag{A.6}$$

In the limit where $\Delta x \to 0$, all three expressions (A.4)–(A.6) will converge to the derivative.

Using standard FDM notation, we write $x_i \equiv x_0 + i\Delta x$ and $\Phi_i \equiv \Phi(x_i)$. Then, if Δx is small but finite, equations (A.4) – (A.6) can be used to obtain approximations of the derivate $\partial_x \Phi$ about the grid point x_i of the form

$$\partial_x \Phi|_{x_i} \approx \frac{\Phi_{i+1} - \Phi_i}{\Delta x} \tag{A.7a}$$

$$\partial_x \Phi|_{x_i} \approx \frac{\Phi_i - \Phi_{i-1}}{\Delta x} \tag{A.7b}$$

$$\partial_x \Phi|_{x_i} \approx \frac{\Phi_{i+1} - \Phi_{i-1}}{2\Delta x}. \tag{A.7c}$$

The three expressions (A.7) are referred to as the ***forward***, ***backward***, and ***centered*** finite difference approximations, respectively, of $\partial_x \Phi$ evaluated at x_i. We shall use the latter in our work.

Now we also need to find a discrete expression for second derivatives. Write (A.1) and (A.2) in terms of the second derivative term:

$$\partial_x^2 \Phi = 2\frac{\Phi(x + \Delta x) - \Phi(x) - \partial_x \Phi \Delta x}{\Delta x^2} + O(\Delta x)$$

$$\partial_x^2 \Phi = 2\frac{\Phi(x - \Delta x) - \Phi(x) + \partial_x \Phi \Delta x}{\Delta x^2} + O(\Delta x).$$

Now adding these two equations, we get

$$\partial_x^2 \Phi = \frac{\Phi(x + \Delta x) - 2\Phi(x) + \Phi(x - \Delta x)}{\Delta x^2} + O(\Delta x). \tag{A.8}$$

Then, taking Δx to be small but finite, we can approximate the second derivate $\partial_x^2 \Phi$ about the grid point x_i:

$$\partial_x^2 \Phi|_{x_i} \approx \frac{\Phi_{i+1} - 2\Phi_i + \Phi_{i-1}}{\Delta x^2}. \tag{A.9}$$

Thus far we have only used three-point stencils to derive all the FDA's, and it turns out sometimes the necessity arises to use a more accurate scheme, such as an FDA based on a five-point stencil (see Fig A.1 on the right). In this case the derivative approximations are more accurate because more nodes are being used (four neighbouring points as opposed to just the two immediate neighbours, as in the previously derived formulæ. Using these extra nodes, we Taylor-expand

$$\Phi(x \pm 2\Delta x) \approx \Phi(x) \pm \partial_x \Phi(2\Delta x) + \partial_x^2 \Phi \frac{(2\Delta x)^2}{2} \pm \partial_x^3 \Phi \frac{(2\Delta x)^3}{6} + \dots \tag{A.10}$$

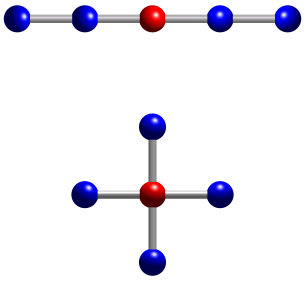

Figure A.1: Five-point stencil in one (top) and two (bottom) dimensions. [Image from Wikipedia]

Substracting the positive and negative versions of this expansion yields

$$\Phi(x + 2\Delta x) - \Phi(x - 2\Delta x) \approx \partial_x \Phi(4\Delta x) + \partial_x^3 \Phi \frac{8\Delta x^3}{3} + \dots \tag{A.11}$$

We can then get rid of the $\partial_x^3\Phi$ term by multiplying $8\times\big((\text{A.1})-(\text{A.2})\big)$ and then substracting (A.11):

$$8\Phi(x+\Delta x)-8\Phi(x-\Delta x)-\Phi(x+2\Delta x)+\Phi(x-2\Delta x)\approx\partial_x\Phi(12\Delta x)+\dots \tag{A.12}$$

This leaves us with an expression for a five-point stencil approximation of the first derivative:

$$\partial_x\Phi\approx\frac{8(\Phi_{i+1}-\Phi_{i-1})-\Phi_{i+2}+\Phi_{i-2}}{12\Delta x}. \tag{A.13}$$

Similar derivations yield five-point stencil FDA's for higher derivatives:

$$\partial_x^2\Phi\approx\frac{16(\Phi_{i+1}+\Phi_{i-1})-30\Phi_i-\Phi_{i+2}-\Phi_{i-2}}{12\Delta x^2} \tag{A.14}$$

$$\partial_x^3\Phi\approx\frac{\Phi_{i+2}-\Phi_{i-2}+2(\Phi_{i-1}-\Phi_{i+1})}{2\Delta x^3} \tag{A.15}$$

$$\partial_x^4\Phi\approx\frac{\Phi_{i+2}+\Phi_{i-2}+6\Phi-4(\Phi_{i+1}+\Phi_{i-1})}{\Delta x^4}. \tag{A.16}$$

We make use of the latter FDA in the von Neumann analysis of our code (§ 2.3).

A.1 Simpson's Method

We need to evaluate, numerically, a double integral

$$S_E=\int_{\tau_{\min}}^{\tau_{\max}}\int_{x_{\min}}^{x_{\max}}\mathcal{L}\,\mathrm{d}x\,\mathrm{d}\tau. \tag{A.17}$$

We will tackle this integration via a 2D Simpson method. In 1D, according to *Simpson's composite* $1/3$ *rule*, an integral

$$I=\int_a^b f(x)\,\mathrm{d}x$$

is approximated by partitioning the interval $[a,b]$ into N evenly spaced segments $a=x_0<x_1<\cdots<x_N=b$ with spacing $\mathrm{h}\equiv(b-a)/N$, and then putting

$$I\approx\frac{\mathrm{h}}{3}\left[f_0+4\sum_{\substack{i=1\\ i\text{ is odd}}}^{N-1}f_i+2\sum_{\substack{i=2\\ i\text{ is even}}}^{N-2}f_i+f_N\right], \tag{A.18}$$

where as usual we wrote $f_k\equiv f(x_k)$, and we point out the requirement that in order for (A.18) to work N must be even. Alternatively, note that we may write this in vector form as

$$I\approx\frac{\mathrm{h}}{3}\boldsymbol{s}\boldsymbol{f}^T, \tag{A.19}$$

where $\boldsymbol{s}=[1\,4\,2\,4\cdots2\,4\,1]$ and $\boldsymbol{f}=[f_0\cdots f_N]$ are vectors of length $N+1$. In the $2D$ extension of this method both $\boldsymbol{s}$ and $\boldsymbol{f}$ become $(N+1)\times(N+1)$ matrices, $\boldsymbol{S}$ and $\boldsymbol{F}$. The latter is the Lagrangian that we want to integrate ($=\mathcal{L}$ in (A.17)), while the fomer is

acquired by multiplying the Simpson coefficients at each grip point; for instance, if $N = 4$,

$$S = \begin{pmatrix} 1\times 1 = 1 & 4\times 1 = 4 & 2\times 1 = 2 & 4\times 1 = 4 & 1\times 1 = 1 \\ 1\times 4 = 4 & 4\times 4 = 16 & 2\times 4 = 8 & 4\times 4 = 16 & 1\times 4 = 4 \\ 1\times 2 = 2 & 4\times 2 = 8 & 2\times 2 = 4 & 4\times 2 = 8 & 1\times 2 = 2 \\ 1\times 4 = 4 & 4\times 4 = 16 & 2\times 4 = 8 & 4\times 4 = 16 & 1\times 4 = 4 \\ 1\times 1 = 1 & 4\times 1 = 4 & 2\times 1 = 2 & 4\times 1 = 4 & 1\times 1 = 1 \end{pmatrix}.$$

The pattern is now clear for general N:

$$S = \begin{pmatrix} 1 & 4 & 2 & 4 & \cdots & 2 & 4 & 1 \\ 4 & 16 & 8 & 16 & \cdots & 8 & 16 & 4 \\ 2 & 8 & 4 & 8 & \cdots & 4 & 8 & 2 \\ 4 & 16 & 8 & 16 & \cdots & 8 & 16 & 4 \\ \vdots & \vdots & \vdots & \vdots & \vdots & \vdots & \vdots & \vdots \\ 2 & 8 & 4 & 8 & \cdots & 4 & 8 & 2 \\ 4 & 16 & 8 & 16 & \cdots & 8 & 16 & 4 \\ 1 & 4 & 2 & 4 & \cdots & 2 & 4 & 1 \end{pmatrix}. \tag{A.20}$$

Thus we approximate the 2D integral (A.17) via the Frobenius inner product [1]

$$S_E \approx \frac{h^2}{9} S \otimes_F \mathcal{L} \equiv \frac{h^2}{9} \sum_{i=\tau_{\min}}^{\tau_{\max}} \sum_{j=x_{\min}}^{x_{\max}} S_{ij}\, \mathcal{L}_{ij}, \tag{A.21}$$

where S_{ij} is understood to be the (i,j)-component of (A.20) and $\mathcal{L}_{ij}$ is the FDA of the Lagrangian $\mathcal{L}$. Our user-defined C++ function for this 2D Simpson implementation is shown on listing A.1.

```
// 2D Simpson's Rule
double Simpson2D (vector<vector<double>> &Fij,  double step_size,
    int taumax,  int xmax){
    // Initialize variables
    vector<double> Si {};
    vector<double> Action_Vec {};
    double actionvals {};
    double Action {};
    double Total_Action {};
    //initialize 2D  vector Sij to have size 121 x 121
    vector<vector<double>> Sij (taumax+1,
    vector<double> ( xmax+1, 0.0 ) );

    for (int i {0}; i <= taumax; i++){
        for (int j {0}; j <= xmax; j++){
            if (i == 0 || i == taumax) {
               if (j == 0 || j == xmax)
                  Sij.at(i).at(j) = 1.0;
               else if (j % 2 != 0)
                  Sij.at(i).at(j) = 4.0;
              else
                  Sij.at(i).at(j) = 2.0;
            }
            else if (j == 0 || j == xmax) {
                 if (i % 2 != 0)
                    Sij.at(i).at(j) = 4.0;
```

[1] This is, of course, assuming the grid spacing h is uniform and equal in both the x and y directions.

```
                else
                    Sij.at(i).at(j) = 2.0;
            }
            else {
                if ( (i % 2 != 0) && (j % 2 != 0) )
                    Sij.at(i).at(j) = 16.0;
                else if ( ((i % 2 != 0) && (j % 2 == 0))
                        || ((i % 2 == 0)
                        && (j % 2 != 0)) )
                    Sij.at(i).at(j) = 8.0;
                else
                    Sij.at(i).at(j) = 4.0;
            }
            actionvals = (Sij.at(i).at(j)) * (Fij.at(i).at(j));
            Si.push_back(actionvals);
        }   //end of main 'j' loop
        Action = accumulate(Si.begin(), Si.end(), 0.0 );
        Action_Vec.push_back(Action);
        Si.clear();
    }    //end of main 'i' loop
    Total_Action = (pow(step_size,2)/9.0) *
             ( accumulate(Action_Vec.begin(),
             Action_Vec.end(), 0.0 ) );
    Action_Vec.clear();

    return Total_Action;
}
```

Listing A.1: Our user-defined 2D Simpson function.

A.2 Least Squares Fitting (LSF)

We begin with a set of n data points $P_0, \ldots, P_{n-1}$, where $P_i = (x_i, y_i)$. The procedure then is to find a line $y = mx + b$ (m being the slope and b the y-intercept) which best fits the data set (note that this is a classical max/min calculus problem). The vertical distance from $Pi = (x_i, y_i)$ to the line $y = mx + b$ is $|y_i - (mx_i + b)|$. However, since we are heading toward a calculus style max/min process, the absolute value is an inconvenience. To get around this, we instead square each of these terms and then add them all to get a function σ which depends on m and b:

$$\sigma(m, b) = \sum_i [y_i - (mx_i + b)]^2. \tag{A.22}$$

Next we apply standard max/min techniques to σ. Differentiating,

$$\frac{\partial \sigma}{\partial m} = \sum_i 2\,[y_i - (mx_i + b)](-x_i) = 2\sum_i [mx_i^2 + (b - y_i)x_i]$$
$$\frac{\partial \sigma}{\partial b} = 2\sum_i [y_i - (mx_i + b)],$$

and then setting these derivatives to zero,

$$0 = \sum_i [mx_i^2 + (b - y_i)x_i] = m\sum_i x_i^2 + b\sum_i x_i - \sum_i x_i y_i$$
$$0 = \sum_i [y_i - (mx_i + b)] = -m\sum_i x_i - nb + \sum_i y_i.$$

Thus we have a a 2×2 linear system with unknowns m and b,

$$\sum_i x_i y_i = m \sum_i x_i^2 + b \sum_i x_i \tag{A.23a}$$

$$\sum_i y_i = m \sum_i x_i + nb, \tag{A.23b}$$

or in matrix notation,

$$\begin{pmatrix} \sum_i x_i^2 & \sum_i x_i \\ \sum_i x_i & n \end{pmatrix} \begin{pmatrix} m \\ b \end{pmatrix} = \begin{pmatrix} \sum_i x_i y_i \\ \sum_i y_i \end{pmatrix}. \tag{A.23⊛}$$

Now, introducing

$$A \equiv \begin{pmatrix} x_0 & \cdots & x_{n-1} \\ 1 & \cdots & 1 \end{pmatrix}$$

it is immediate that

$$AA^T = \begin{pmatrix} x_0 & \cdots & x_{n-1} \\ 1 & \cdots & 1 \end{pmatrix} \begin{pmatrix} x_0 & 1 \\ \vdots & \vdots \\ x_{n-1} & 1 \end{pmatrix} = \begin{pmatrix} \sum_i x_i^2 & \sum_i x_i \\ \sum_i x_i & n \end{pmatrix},$$

and

$$A \begin{pmatrix} y_0 \\ \vdots \\ y_{n-1} \end{pmatrix} = \begin{pmatrix} \sum_i x_i y_i \\ \sum_i y_i \end{pmatrix}.$$

Hence we may rewrite the 2×2 system (A.23⊛) as

$$AA^T \begin{pmatrix} m \\ b \end{pmatrix} = A \begin{pmatrix} y_0 \\ \vdots \\ y_{n-1} \end{pmatrix}. \tag{A.23⊛}$$

We then use a numerical package to solve this linear system; in our work we used **Numpy**, in which the built-in function **`numpy.linalg.lstsq`** suffices (see listing A.2).

```
import pandas as pd
import numpy as np

#import data using panda
x_pd = pd.read_csv("~/PATH to lambda csv. file", header = None)
y_pd = pd.read_csv("~/PATH to alpha csv. file", header = None)

#convert panda data to numpy data
x = np.array(x_pd[0])
y = np.array(y_pd[0])

#define A transpose
Atr = np.vstack([x, np.ones(len(x))]).T

#get slope m and y-intercept b (from y = mx + b)
m, b = np.linalg.lstsq(Atr, y, rcond=None)[0]
```

Listing A.2: Linear LSF code to get the line $y = mx + b$ that best fits our data of α as a function of λ.

For the sake of completion let us just point out that the generalisation of the above procedure to a fitting with an m-degree polynomial is straightforward. The coefficient matrix A takes the form

$$A \equiv \begin{pmatrix} x_0^m & \cdots & x_{n-1}^m \\ \vdots & \vdots & \vdots \\ x_0 & \cdots & x_{n-1} \\ 1 & \cdots & 1 \end{pmatrix},$$

and instead of two independent variables m and b, we have $m+1$ variables $a_0, \ldots, a_m$, so that

$$AA^T \begin{pmatrix} a_m \\ \vdots \\ a_0 \end{pmatrix} = A \begin{pmatrix} y_0 \\ \vdots \\ y_{n-1} \end{pmatrix}. \qquad (A.23\circledcirc)$$

The concept of LSF extends well beyond polynomials. For instance, we may also apply a LSF to our ansatz (3.7) from Chapter 2,

$$S_E = \frac{\alpha}{T}.$$

Applying the same procedure as above, we start from a function σ which depends only on α:

$$\sigma(\alpha) = \sum_i \left(y_i - \frac{\alpha}{x_i} \right)^2,$$

where the x_i are the temperature (T) values and y_i are the action (S_E) values on our data. Next we apply standard $\max/\min$ techniques to σ. Differentiating,

$$\frac{\partial \sigma}{\partial \alpha} = \sum_i 2 \left(y_i - \frac{\alpha}{x_i} \right) \left(-\frac{1}{x_i} \right) = 2 \sum_i \left(\frac{\alpha}{x_i^2} - \frac{y_i}{x_i} \right)$$

and now setting to zero,

$$0 = 2 \sum_i \left(\frac{\alpha}{x_i^2} - \frac{y_i}{x_i} \right) \implies \sum_i \frac{y_i}{x_i} = \sum_i \frac{\alpha}{x_i^2},$$

we find α from the equation

$$\alpha = \frac{\sum_i \frac{y_i}{x_i}}{\sum_i x_i^{-2}},$$

which is precisely Equation (3.8) that we used on Chapter 2. For this LSF there is no need to use some numerical package, since there is no matrix multiplication/inversion involved. Our own code to find α is shown on listing A.3.

```
// functor for getting sum of previous result and square inverse of
    current element
template<typename T>
struct invsqr{
    T operator()(const T& Left, const T& Right) const{
        return (Left + pow(Right*Right, -1) );
    }
};

// S_E = alpha/T
```

```
10 double S_Ansatz (vector <double> temp, vector <double> action){
11
12     // Initialize variables
13     double xval_invsqr {};
14     double yval_over_xval {};
15     vector <double> y_over_x {};
16     double alpha {};
17
18     for (int i{0}; i <= temp.size()-1; i++) {
19         y_over_x.push_back( (action.at(i))/(temp.at(i)));
20     }
21
22     yval_over_xval = accumulate(y_over_x.begin(), y_over_x.end(), 0.0 )
       ;
23     y_over_x.clear();
24     xval_invsqr = accumulate(temp.begin(), temp.end(), 0.0, invsqr<
       double>() );
25
26     alpha = yval_over_xval/xval_invsqr;
27     return alpha;
28 }
```

Listing A.3: LSF for ansatz (3.7) to determine α.

Bibliography

[AH92] Anderson, G. W. and Hall, L. J. "Electroweak phase transition and baryogenesis". In: *Phys. Rev. D* vol. 45 (8 Apr. 1992), pp. 2685–2698.

[AM20] Abed, M. G. and Moss, I. G. "Bubble nucleation at zero and nonzero temperatures". In: (June 2020). arXiv: 2006.06289 [hep-th].

[Bil+19] Billam, T. P. et al. "Simulating seeded vacuum decay in a cold atom system". In: *Phys. Rev. D* vol. 100 (6 Sept. 2019), p. 065016.

[Bra+19] Braden, J. et al. "New Semiclassical Picture of Vacuum Decay". In: *Phys. Rev. Lett.* vol. 123 (3 July 2019), p. 031601.

[Cap+09] Caprini, C. et al. "General Properties of the Gravitational Wave Spectrum from Phase Transitions". In: *Phys. Rev.* vol. D79 (2009), p. 083519. arXiv: 0901.1661 [astro-ph.CO].

[CC77] Callan, C. G. and Coleman, S. "Fate of the false vacuum. II. First quantum corrections". In: *Phys. Rev. D* vol. 16 (6 Sept. 1977), pp. 1762–1768.

[Col77] Coleman, S. "Fate of the false vacuum: Semiclassical theory". In: *Phys. Rev. D* vol. 15 (10 May 1977), pp. 2929–2936.

[DV17] Deng, H. and Vilenkin, A. "Primordial black hole formation by vacuum bubbles". In: *JCAP* vol. 1712, no. 12 (2017), p. 044. arXiv: 1710.02865 [gr-qc].

[Fia+15] Fialko, O. et al. "Fate of the false vacuum: Towards realization with ultra-cold atoms". In: *EPL (Europhysics Letters)* vol. 110, no. 5 (June 2015), p. 56001.

[Hin+14] Hindmarsh, M. et al. "Gravitational waves from the sound of a first order phase transition". In: *Phys. Rev. Lett.* vol. 112 (2014), p. 041301. arXiv: 1304.2433 [hep-ph].

[HMS82] Hawking, S. W., Moss, I. G., and Stewart, J. M. "Bubble Collisions in the Very Early Universe". In: *Phys. Rev.* vol. D26 (1982), p. 2681.

[Lin83] Linde, A. D. "Decay of the False Vacuum at Finite Temperature". In: *Nucl. Phys. B* vol. 216 (1983). [Erratum: Nucl.Phys.B 223, 544 (1983)], p. 421.

[LV16] Laine, M. and Vuorinen, A. *Basics of Thermal Field Theory*. Vol. 925. Springer, 2016. arXiv: 1701.01554 [hep-ph].

[MR17] MÃ©gevand, A. and RamÃrez, S. "Bubble nucleation and growth in very strong cosmological phase transitions". In: *Nuclear Physics B* vol. 919 (2017), pp. 74–109.